RSC Advances

PAPER

View Article Online
View Journal | View Issue

Cite this: *RSC Adv.*, 2022, **12**, 22119

Synthesis and characterization of tung oil-based UV curable for three-dimensional printing resins†

Zicheng Zhao,[ab] Hong Wu,[b] Xudong Liu,[b] Desheng Kang,[c] Zhihong Xiao,[b] Qiquan Lin*[a] and Aihua Zhang*[b]

Using tung oil as the raw material, a new bio-based prepolymer was successfully synthesized by reacting with acrylic-modified rosin (β-acryloyl nutrient ethyl) ester (ARA)/acrylic-2-hydroxyethyl ester (HEA) followed by the use of the above composite material as the matrix and then reacting with the active diluent (2-HEMA, TPGDA) and the photoinitiator TPO and Irgacure1173 to successfully synthesize a new type of bio-based prepolymer-acrylate-epoxy tung oil polypolymer (AETP). The tung oil monomer before and after the epoxy formation was compared by proton NMR spectroscopy, and the chemical structure of AETP was analyzed by Fourier transform spectroscopy. Tung oil has an acid value of 1.5 mg KOH per g, an epoxy value of 5.38%, an iodine value of 11.28 g/100 g, and a refractive index of $n^{25} = 1.475$. Composite-based 3D printing resins (like AETP) were cured using digital light treatment, while some samples were also post-treated *via* ultraviolet (UV) light treatment. The AETP-based 3D printing resin has excellent thermal and mechanical properties, and the viscosity of its system is 313 mPa s; exposure time 4.5 s; the tensile strength, flexural strength and flexural modulus were 62 MPA, 63.84 MPa and 916.708 MPa, respectively; Shore hardness was 80 HD and shrinkage was 4.00%. The good performance of the AETP-based 3D printing resin is attributed to the rigidity of their tightly crosslinked structure. This study pioneered a method for producing photoactive acrylates (*e.g.*, tung oil-based acrylate oligomer resins) from renewable, low-cost biomass for light-curing 3D printing.

Received 24th May 2022
Accepted 19th July 2022

DOI: 10.1039/d2ra03182e

rsc.li/rsc-advances

1. Introduction

Three-dimensional (3D) printing has revolutionized product design and manufacturing since its inception. The advantage of 3D printing is that it has higher precision, convenience, speed, and lower environmental impact compared to the traditional mold casting technology.[1]

In recent years, the 3D printing technology based on light curing has developed rapidly. Numerous processes, including direct ink writing (DIW), selective laser sintering (SLS), stereolithography equipment (SLA), digital light processing (DLP), and continuous liquid interface production (CLIP), have been developed to meet a variety of requirements.[2] The applicability of this technology continues to expand and it is currently used in healthcare, aerospace, automotive, food industry, art, textiles and fashion, and construction. This technology has revolutionized the manufacture and development of products and has attracted widespread attention around the world.[3]

The most widely used light-curing 3D printing materials typically consist of acrylic oligomers, including epoxy acrylates, polyesters, polyethers, polyurethanes, and silicones.[4] They have the advantages of fast curing and low energy consumption.[5–7] However, there are plenty of challenges to overcome before light-curing-based 3D printing technology can be effectively implemented as a common manufacturing technique.[8] Materials used in light-curing-based 3D printing must have a low environmental impact while being compatible with light-curing printers, which hinders the large-scale application of the technology.[9] Therefore, in numerous light-curing-based 3D printing applications, the development of biomass-based materials to replace petroleum-based prepolymers offers potential for a truly sustainable circular economy.[10] Bio-based materials, from the ocean,[11] wood,[12–14] agricultural residues,[15,16] are the most abundant renewable raw materials on the earth, and have shown great potential to replace fossil fuels.

The main component of tung oil is tung oleic acid (>80%), which contains 3-member conjugated double bonds and carboxyl groups and other active groups in its structure, which has strong chemical reaction activity and derivatization potential. Free radical polymerization[17,18] and cationic polymerization can also occur under the condition of UV light, especially in light-curing coatings,[19,20] and it has been found that when tung oil is added at 20%, together with 50% epoxy, 25% active diluent

[a]*College of Mechanical Engineering and Mechanics, Xiangtan University, Xiangtan 411105, China. E-mail: xtulqq@163.com*

[b]*State Key Laboratory of Utilization of Woody Oil Resource, Hunan Academy of Forestry, Changsha 410000, China. E-mail: zhangaihua909@163.com*

[c]*Hunan Xiangchun Agricultural Technology Co., Ltd, Changsha 410000, China*

† Electronic supplementary information (ESI) available. See https://doi.org/10.1039/d2ra03182e

acryloyl morpholine, 5% triaryl thiol salt and 1% free radical photoinitiator benzoin diethyl ether, the film light curing rate is 93.25%, and the mechanical properties are excellent.[21]

In addition, tung oil can also be used to prepare plastics,[22,23] biodiesel,[24] microcapsules,[25] *etc.* Tung oil can also be used as a resin-modified matrix, mixed with other raw materials *via* chemical modification to prepare tung oil-based coatings.[26] The annual output of tung oil in China is more than 100 000 tons, accounting for 80% of the world's tung oil production. Tung oil-based products have the characteristics of good adhesion, strong water resistance, and excellent electrical insulation,[27] and have been widely used in the modification of synthetic resins. The level of utilization technology of tung oil in China is low, and past research has mainly focused on the direct use of tung oil as an anti-corrosion coating, ink additive, or release oil; or its boiling mature oil as a rain gear tarpaulin coating, waterproofing and anti-rust coating for steel components, and varnish and insulating varnish.[28] These uses are generally achieved by the oxygen polymerization reaction of the 3-member conjugated double bond in tung oil, the resulting material has strong brittleness, greatly affecting the durability and use performance of the material, if you can use the active group contained in tung oil, through the Diel–Alder reaction,[29,30] Friedel–Crafts reaction,[31] epoxidation, amidation and esterification, and other chemical reactions through the introduction of more reactive reaction groups. In addition, the molecular structure and size are designed through atomic transfer radical polymerization, which can not only greatly improve the brittleness of tung oil-based products but also increase the added value of tung oil products and further expand the scope for the use of tung oil.[32] In recent years, with the increase in the depletion of petrochemical resources, renewable resources have attracted the attention of various countries. The use of China's rich tung oil resources to develop tung oil downstream products has great practical significance in today's era of increasing shortage of petrochemical resources.[33]

To date, significant research has been conducted on the development of tung oil light curing, a process that uses photosensitive tung oil as a light curing material. However, the light curing of tung oil oligomers for 3D printing has rarely been reported. To evaluate the potential application of tung oil-based acrylates in the field of 3D printing, we prepared acrylate-epoxy tung oil polypolymers (AETPs) and analyzed their properties using chemical and spectroscopic methods. The AETP-based 3D printing resin with excellent printing performance was prepared. In general, 3D products printed using AETP have excellent thermal and mechanical properties. The good material properties exhibited by bio-based AETP resins demonstrate the utility of photoactive acrylates over a wide range of applications.

2. Experimental

2.1 Raw materials

Tung oil was obtained from Guosheng Bioenergy Co., Ltd. in Chenzhou City, Hunan Province. Acrylic modified rosin (β monoacryloyloxyethyl) ester (ARA), synthesized according to literature,[34] *n*-butanol, absolute ethanol, 2-hydroxyethyl methacrylate (HEMA), hydroquinone, xylene, H_2O_2, formic acid, NaCl solution, tripropylene glycol diacrylate (TPGDA) and 2,4,6-trimethylbenzoyldiphenylphosphine (TPO) were purchased from Aladdin Industries. Photoinitiator 2-hydroxy-2-methyl-1-phenyl-1-acetone (trade name Irgacure1173), ACROS, and all other materials were used as-received without further purification.

2.2 Preparation of tung oil-based photosensitive monomers

2.2.1 Mechanism of epoxygenation. Under certain conditions, greases containing unsaturated bonds can react with peroxy acids to form an oxygenated ternary ring on the carbon–carbon double bond. There are various ways to form peroxy acids, and oxygen and hydrogen peroxide were used as oxygen sources or peroxide reagents were directly added to the reaction system. With H_2O_2 as the oxygen source of "instantaneous preparation of peroxy acid", hydrogen peroxide and formic acid form formic acid peroxide under the action of the catalyst, and the generated peroxycarboxylic acid immediately reacts with the unsaturated bond in the oil, and the reactive oxygen species is transferred to the unsaturated 1 bond to form an epoxy group; the epoxidation reaction mechanism is as follows (Fig. 1).

2.2.2 Preparation of epoxy greases. A certain amount of tung oil was taken in a 300 mL round bottom flask, and then a certain amount of formic acid was added to the flask. The flask was placed on a constant temperature magnetic stirrer under slow stirring. The water bath was heated to a specified temperature; after the temperature was reached, the contents were stirred rapidly, while adding 130–160% (grease mass fraction) hydrogen peroxide (30%, the safety note about the use of hydrogen peroxide is on the Pages S2–S15 in the ESI†), which needed to be dropwise added within 1 h. After the dropwise addition was completed, the water bath was heated to the required reaction temperature of 50–60 °C, the start timing was noted and the reaction was maintained for a certain time. After the reaction was over, the contents were centrifuged and separated at room temperature, the upper oil layer was taken and transferred to a pear-shaped separating funnel, and then washed with saturated NaCl solution at room temperature until the lower aqueous solution was neutral. After washing, the oil sample was transferred to a round bottom flask, and the remaining water and low boiling point substances were removed by distillation at 85–95 °C under reduced pressure, and the epoxy tung oil was obtained.

2.3 Preparation of UV-curable composites based on tung oil

The epoxy tung oil was mixed with the active diluents HEA, ARA, and photoinitiator according to the proportions given in Table

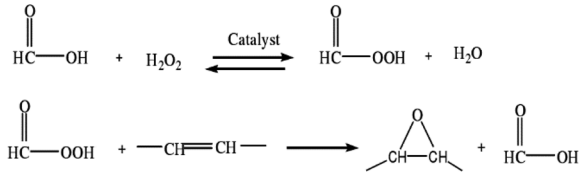

Fig. 1 Mechanism of epoxygenation.

1, and 5 groups of ultraviolet curable paint samples were prepared, coated into a film at 25 μm, and light cured at a distance of 5 cm. Subsequently, one of the sets of samples was prepared by homogeneously mixing one of the samples with the reactive diluent (2-HEMA, TPGDA) and the photoinitiators TPO and Irgacure1173. The recipes are shown in Table 2.

2.4 Preparation of AETP resin based on UV curing materials

3D architecture used was a commercial Lite600HD 3D printer (Shanghai Luen Thai Technology Co., Ltd.). Solidworks 2018 modeling software was used to create samples for bending, tensile, and impact performance testing. The specimen was prepared according to the sample size specified in the national model standards, such as GB/T 1040.2-2006, GB/T 9341-2000, and GB/T 1843-2008. The file was saved in the STL format, imported into a 3D printer, and printed using the prepared photosensitive resin. The 3D printed product was soaked in an anhydrous ethanol bath for 5 min to remove any unreacted substances and then dried under ambient conditions.

2.5 Characterization

2.5.1 Epoxide value. Referring to GB/T1677-2008, the hydrochloric acid-acetone method was used for the epoxy value determination, the specific operation process is as follows: hydrochloric acid and acetone were configured according to 1 : 40 (volume ratio), shaken well, and placed in the reagent bottle, capped and set aside. A certain amount of NaOH was weighed, and 95% ethanol was used to prepare a 0.1 mol L^{-1} NaOH ethanol solution, which was shaken well and placed into the reagent bottle, and the lid was covered for later use. The above solution should be used quickly to avoid its deterioration. A 0.5 g of the sample was taken into a clean Erlenmeyer flask, and 20 mL of the prepared hydrochloric acid-acetone solution was slowly added; the solution was covered and shaken thoroughly until it was uniform for about 0.5–1 h. Five drops of phenolphthalein were added and the added NaOH ethanol solution was titrated until the solution was light pink, and the color did not fade within 30 s. Two blank titrations were performed according to the above method.

$$E = \frac{(V - V_1)c}{10m}$$

E: epoxide value, mol/100 g;

V: blank experiments consumed the average volume of NaOH ethanol solution, mL;

Table 1 Ratio of tung oil with ARA/HEA coatings

Samples	Epoxy tung oil (g)	ARA (%)	HEA (%)	1173 (%)
1#	20	97	0	3
2#	20	87	10	3
3#	20	77	20	3
4#	20	67	30	3
5#	20	57	40	3

V_1: the titration of the sample taken consumes the volume of NaOH ethanol solution, mL;

c: molar concentration of NaOH ethanol solution, mol L^{-1};

m: the weight of the specimen, g.

2.5.2 ^{1}H NMR. An Avance III.400 MHz Superconducting Fourier NMR spectrometer (Bruker Corporation, Germany) was used for measurements at room temperature, and the solvent was deuterium chloroform ($CDCl_3$). The double bond content was tested using the ^{1}H NMR internal standard method, and the sample and 1,4-dioxane were mixed with the deuterated chloroform solvent during the sample preparation, and the double bond content (DB) was calculated according to the formula mentioned below after ultrasonic testing.[35]

$$\mathrm{DB} = \frac{\frac{A}{3} \times w_{\mathrm{standard}}}{\frac{B}{8} \times w_{\mathrm{sample}} \times 88} \times 100\%$$

DB: molar fraction of double bonds in 100 g sample, mol/100 g;

w_{standard}: mass of 1,4-dioxane, g;

w_{sample}: the weight of the specimen, g;

88 is the relative molecular mass of 1,4-dioxane, g mol^{-1};

8 is the number of H protons for 1,4-dioxane;

3 is the number of H protons for the double bond;

A is the peak area of double bond NMR absorption;

B is the peak area of the methylene NMR in 1,4 dioxane.[35]

2.5.3 FT-IR. Fourier transform infrared spectroscopy (FT-IR) analysis was performed using a QuestGS10800 spectrometer (Specac, UK) using the KBr tablet method. The test scan range was between 4000 and 500 cm^{-1}, with a spectral resolution of 4 cm^{-1}.[36]

2.5.4 Gel content. ASTMD2765-2016 test standard method was followed. A certain amount of printing material was added to the glass dish with a mass of M_0, the thickness was about 3 mm, and the total mass at the weighing is denoted as M. The glass dish was placed under a UV lamp and removed at a fixed time of 40 (s), soaked in xylene solvent for 24 h, dissolved, and the uncured surface was removed from the printing material, wiped clean, and placed in the drying box at 140 °C for volatile curing of the film surface by the solvent. The mass of the resin M_1 was weighed and recorded after curing and molding. Calculated according to the formula: $\frac{M_1}{M - M_0} \times 100\%$.

2.5.5 Water contact angle. A DSAl00 contact instrument was used (Kruss, Shanghai). The 5 samples were dissolved thoroughly, and after each sample expanded and stabilized on the glass substrate, the water contact angle of each sample was tested on the glass.

2.5.6 Thermogravimetric analysis (TGA). A TGA/DSC 3+ thermogravimetric instrument (Mettler-Toledo, Switzerland) was used. The test conditions were as follows: an N_2 atmosphere (flow rate 20 mL min^{-1}), a heating rate of 20 °C min^{-1} at a heating range between 40 and 800 °C.

2.5.7 Coating adhesion and pencil hardness. The coating adhesion test was performed using an adhesion tester (Tianjin

Table 2 Formulations of photosensitive AETP resin

Formulation	Composites (wt%)	2-HEMA (wt%)	TPGDA (wt%)	TPO (wt%)	1173 (wt%)
AETP-1	55	20	20	3	2
AETP-2	65	15	15	3	2
AETP-3	75	10	10	3	2

Shiboweiye Glass Instrument Co., Ltd., China). According to the procedure specified in GB1720-79 (89), the adhesion level was allocated a value between 1 (best) and 7 (worst). The pencil hardness test was performed using a QHQ-A pencil hardness tester (Tianjin Litengda Instrument Co., Ltd., China). The GB/T 6739-1996 guidelines denote the hardness using the following notation: 6H, 5H, 4H, 3H, 2H, H, HB, B, 2B, 3B, 4B, 5B, or 6B (where 6H is the hardest and 6B is the softest).

2.5.8 DMA. Dynamic mechanical analysis (DMA) was performed using a TA Instruments (USA) DMA Q800. DMA tests were performed between −50 and 100 °C at a heating rate of 2 °C min^{-1} at 1 Hz.

2.5.9 Viscosity-shear rate. A MCR302 (Anton Paar Corporation, Austria) rheometer was under rotation mode, and the shear rate range was set to 0.1–100 s^{-1}. A rotor of model PP25 was selected to test and record the flow viscosity of resins in different proportions over this shear rate range.[37]

2.5.10 Tensile strength and elongation at break. According to the ASTMD638-2014 standard, a computerized tensile testing machine was selected to install a tensile test module. The type of test strip is I barbell type, thickness (7 ± 0.4) mm. The testing machine fixture was set to load at a tensile rate of 5 [0.2] ± 10% mm min^{-1}, and test the same test strip 5 times. Tensile strength, elongation at break, stress, and strain changes were recorded with the tensile process in the event of a test strip break.

3. Results and discussion

3.1 Results and analysis of the influence of univariate factors on the epoxidation reaction of tung oil

3.1.1 Effect of temperature on the epoxidation reaction of tung oil. Experimental conditions: the amount of formic acid added was 20% of the oil mass, the amount of hydrogen peroxide was 130% of the oil mass, and the reaction time was 4.5 h.

The results are shown in Fig. 2(a): temperature has a more obvious impact on tung oil epoxidation. As the reaction temperature increases, the epoxy value of tung oil increases first; when the reaction temperature reaches 60 °C, the epoxy value reaches the maximum; as the temperature continues to rise, epoxy value begins to decline. The reason is that when the temperature is low, the oil epoxy rate is low, while the increase in temperature will promote the epoxidation reaction. When the temperature is higher, the side reactions will occur in the reaction system, so that the ring-opening reaction rate in the oil system is accelerated, and at this time, the reaction rate of the oil ring-opening reaction in the system is greater than the epoxidation reaction rate, and the solid epoxy value is reduced. Therefore, considering the analysis, the most suitable reaction temperature for tung oil epoxidation is 60 °C.

3.1.2 Effect of time on the epoxidation reaction of tung oil. Experimental conditions: the amount of formic acid added was 20% of the oil mass, the amount of hydrogen peroxide was 130% of the oil mass, and the reaction temperature was 60 °C.

The results are shown in Fig. 2(b): as the reaction time gradually increases, the epoxy value of tung oil increases first; when the reaction time reaches 4.5 h, the epoxy value of tung oil reaches the maximum; and as the reaction time continues to extend, the epoxy value of tung oil continues to decrease.

Because in the autocatalytic reaction system, as the reaction is carried out, the epoxy bonding is gradually increased, the hydrogen peroxide concentration gradually decreases with the reaction and a large amount of free formic acid is gradually generated;[38] after a certain period of time, in the reaction system, the epoxy oil ring opening side reaction occurs, and at this time, the oil ring opening reaction rate is greater than the epoxy reaction rate, and the epoxy value of the solid tung oil continues to decrease, and the most suitable epoxy reaction time in the process of the tung oil epoxidation reaction in the self-catalytic system can be obtained at 4.5 h.

3.1.3 Effect of formic acid addition on the epoxidation reaction of tung oil. Experimental conditions: the amount of hydrogen peroxide added is 130% of the oil mass, the reaction temperature is 60 °C, and the reaction time is 4.5 h.

The results are shown in Fig. 2(c): as the amount of formic acid is added, the epoxy value shows at first an increasing trend

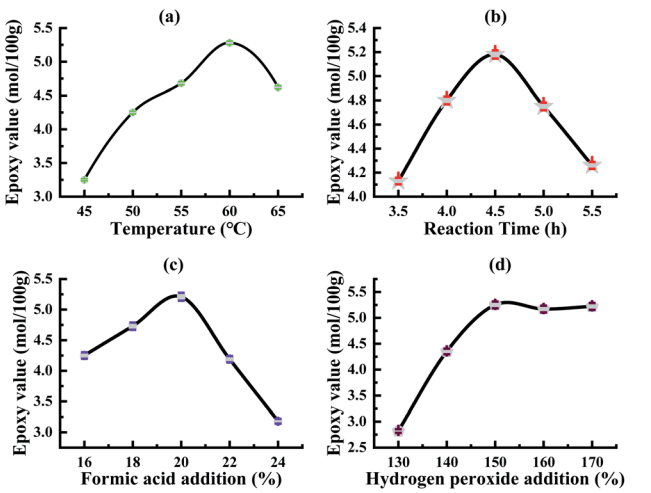

Fig. 2 Effects of different factors on the extraction rate. (a) Reaction temperature, (b) reaction time, (c) the amount of formic acid added, (d) the amount of hydrogen peroxide added.

and then decreasing, and the epoxy value reaches the maximum when the amount of formic acid added (the mass percentage of tung oil) is 20%. As the amount of formic acid added continues to increase, the epoxy value becomes smaller due to the excessive amount of formic acid added, resulting in too much free formic acid being produced in the reaction system, so that the ring opening reaction of epoxy grease is accelerated; when the ring opening rate is greater than the epoxy rate, the tung oil epoxy value decreases; hence, the analysis shows that the most suitable formic acid addition amount is 20%.

3.1.4 Effect of hydrogen peroxide addition on the epoxidation reaction of tung oil. Experimental conditions: the amount of formic acid added is 20% of the oil mass, the reaction temperature is 60 °C, and the reaction time is 4.5 h.

The results are shown in Fig. 2(d): the epoxy value of the obtained oil by the tung oil epoxidation reaction varies significantly with the different amounts of hydrogen peroxide added, and in the tung oil epoxidation autocatalytic reaction system, with the increase in the amount of hydrogen peroxide, the epoxy value of the tung oil epoxidation reaction gradually reaches equilibrium and stabilizes after the rapid growth of the epoxidation reaction. Because the amount of hydrogen peroxide added at the initial stage is relatively small, the content of peroxyformic acid in the autocatalytic reaction system is low, which generates a large amount of free formic acid in the reaction system, which will aggravate the side reactions in the reaction, thereby reducing the epoxy rate. Moreover, when the amount of hydrogen peroxide is continuously increased, the amount of hydrogen peroxide added increases to 150% of the oil mass, and the epoxy value reaches the maximum value and then tends to be stable. When the amount of formic acid is a certain value, the amount of peroxide generated in the system remains unchanged. As such, the analysis can be seen that the optimal hydrogen peroxide addition amount is 150% (oil mass fraction).

Based on the above experiments and the analysis of the results, it can be seen that the optimal reaction conditions for the tung oil epoxidation reaction in the autocatalytic reaction system are: the temperature of 60 °C, reaction time of 4.5 h, amount of formic acid as 20% (oil mass percentage) and amount of hydrogen peroxide as 150% (oil mass percentage).

3.2 Optimization of the epoxidation reaction process of tung oil by the response surface method

See Pages S16–S20.†

3.3 Characterization and performance analysis of epoxy greases

3.3.1 Characterization of epoxy greases

3.3.1.1 Nuclear magnetic analysis. From Fig. S4,† it can be seen that the absorption peak at 5.0–5.5 ppm belongs to the hydrogen atom on the tung oil conjugate double bond. The absorption peak at 4.0–4.5 ppm is due to the chemical displacement of the hydrogen in –CH–O–. The absorption peak at around 3.1 ppm is the characteristic absorption peak of the generated epoxy group. The absorption peak at 2.0–2.2 ppm is due to the chemical shift of the hydrogen in CH_2–C=C. The absorption peak at 2.4 ppm is the chemical displacement of the O=C–CH_2– hydrogen. The absorption peak at 1.2–1.3 ppm is due to the chemical displacement of –CH_2–hydrogen, and that at 1.6 ppm is due to the chemical displacement of the –CH_2–C=C=C– hydrogen. The absorption peak near 0.9 ppm is due to the chemical shift of –CH_3. It can be seen that before the tung oil reaction and after the epoxidation reaction, the hydrogen on the double bond and the hydrogen displacement on the carbon near the double bond have changed; the hydrogen absorption peak due to the double bond of tung oil before the reaction appears at 5.36 ppm and the absorption peak of epoxy tung oil disappears at this location after the epoxy reaction. The hydrogen absorption peak corresponding to the new epoxy bond appears at 3.12 ppm, and the hydrogen displacement on the other bonds does not change, which indicates that the carbon–carbon double bond is generated after the hydrogen-catalytic reaction of hydrogen peroxide–formic acid.[38]

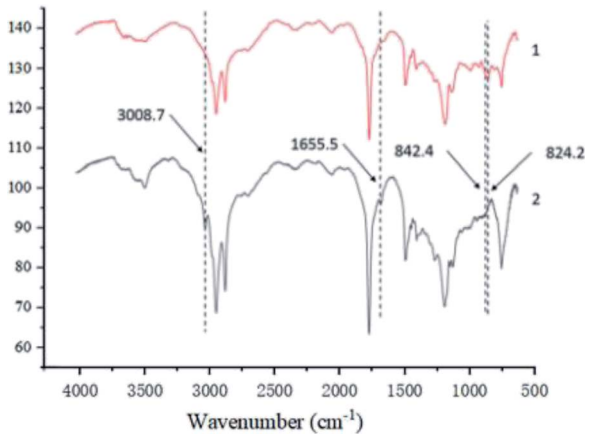

Fig. 3 Infrared spectra before and after tung oil epoxidation.

3.3.1.2 Infrared spectral analysis. Fig. 3 shows the amplified vibration absorption peak of the carbon–hydrogen bond in the carbon–carbon double bond at the 3008.7 cm^{-1} and the carbon–carbon double bond telescopic vibration absorption peak at the 1655.5 cm^{-1} in epoxy tung oil has basically disappeared, it can also be seen from the spectra that the epoxy tung oil has generated a ternary cyclic ether C–O–C asymmetric *cis*-C asymmetric telescopic vibration absorption peaks at the position of 24.2 cm^{-1} and 842.4 cm^{-1}, which can indicate that the tung oil has undergone epoxidation reaction and the target epoxy tung oil has been generated, consistent with the results of MRI characterization.

3.3.2 Physicochemical performance analysis. The physical and chemical properties of tung oil are shown in Table 3; the acid value of tung oil after the epoxy was 1.5 mg KOH per g, the value of epoxy is 5.38%, the value of iodine is 11.28 g/100 g, and the refractive index $n^{25} = 1.475$.

3.4 Characterization of tung oil-based UV-curable materials

3.4.1 Infrared spectral analysis. Fig. S5† is the infrared spectrum of the 3# formulation from Table 1 at different

Table 3 Performance of tung epoxy oil

Acid (mg KOH per g)	Epoxy value (g/100 g)	Iodine value (gI_2/100 g)	Refractive index (25 °C)
1.5	5.38	11.28	1.475

reaction times; 1723 cm^{-1} and 1636 cm^{-1} are the telescopic vibration peaks of C=O of the acrylate group and the C–H telescopic vibration peaks in CH=CH, respectively, of which the C–H telescopic vibration peaks in CH=CH are the reaction peaks and the telescopic vibration peaks of C=O are reference peaks. As can be seen from Fig. S5,† the characteristic vibration of the C=C double bond located at the 1636 cm^{-1} position gradually decreases with the extension of the curing time, and only one C=C double bond absorption peak can be observed at 240 s, indicating that the curing reaction is basically complete.

3.4.2 Analysis of the gel content. Fig. 4 is the degree of crosslinking at different HEA contents, it can be seen that with the increase in the curing time, the gel content increases. With the addition of HEA, the advantage of HEA on the reduction of the viscosity of the system is fully displayed. However, when the HEA content continues to increase, HEA was exhibited as a relatively slow and non-crosslinking nature of the monomer reaction, thus affecting the overall gel content. The effect of HEA on the degree of curing of tung acrylate oil was not that the more HEA content was better, but reflects an optimal amount of addition, and the gel content of the system is the highest when the content of HEA is 20%. The final gel content reached 92.3%.

3.4.3 Water contact angle analysis. The uncured composite material was dripped on the clean and smooth glass surface, the measured contact angle graphic is shown in Fig. S6,† and the specific contact angle values are listed in Table 4. From Table 4, it can be seen that the contact angle value of the composite material is less than 50° and with the increase in the HEA content, the contact angle value of the system on the substrate glass decreases, and the surface wetting performance becomes better. This is mainly due to the strong polar hydroxyl group in HEA, which can form a hydrogen bond effect with the hydroxyl group on the glass surface. On the other hand, there is good compatibility between HEA and ARA, and HEA acts as a wetting aid, and with the increase in the HEA dosage, the wetting performance of the paint increases.

Table 4 Water contact angle values of samples 1#–5#

Series	Left contact angle/degrees	Right contact angle/degrees	Average contact angle/degrees
1#	46.37	48.22	47.23
2#	36.41	36.23	36.17
3#	29.27	29.16	28.97
4#	19.91	19.46	19.91
5#	18.83	18.02	18.15

3.4.4 TG analysis. Fig. 5 shows the thermal weight loss curve of the composite material. The curves begin to lose weight around 100 °C, which is caused by the volatilization of some neutrals of low and medium boiling points in ARA. There are three inflection points in the thermal weight loss curve of formula 1# and formula 2#, which are located at 164.8 °C, 181.9 °C, 356.4 °C, 368.6 °C and 457.1 °C, 452.9 °C, respectively; 3#, 4# and 5# formulas have only one inflection point of 457.8 °C, 448.7 °C, and 456.1 °C, respectively. This may be due to their similar gel content, and weight loss caused by thermal decomposition in the mildly crosslinked parts of the coating. From the changing trend of the entire thermogravimetric loss curve in Fig. 5, it can be seen that the thermogravimetric stability of the 5# formula is the best, followed by those of 3# and 4#, which is consistent with the gel containment analysis results shown in Fig. 4. This may be due to the addition of monofunctional HEA, which reduced the viscosity of the system, and when crosslinked with ARA, the gel amount increases, resulting in good thermal stability. However, the increase in HEA indicates that the amount of ARA used in the bifunctionality is reduced, and the crosslinking point of the coating is reduced, resulting in a decrease in thermal stability. From the analysis results of Fig. 5, it can be concluded that the amount of HEA in experimental recipes 3#, 4# and 5# was moderate.

3.4.5 Effect of HEA content on the mechanical properties of composite materials. In the formulation shown in Table 1,

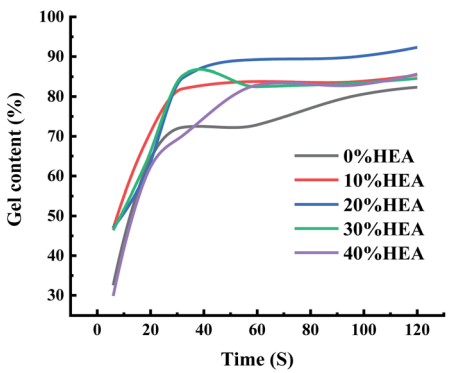

Fig. 4 Effect of HEA content on gel content.

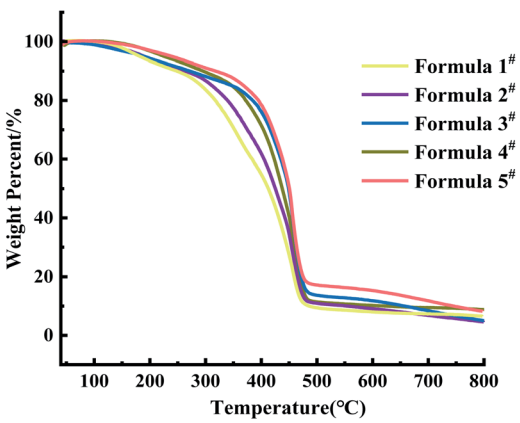

Fig. 5 Effect of HEA content on the thermal weight loss rate of composite materials.

Table 5 Properties of composites with different HEA contents

Series	Content of HEA/%	Adhesion/degree	Pencil hardness
1#	0	3	3H
2#	10	2	3H
3#	20	1	2H
4#	30	1	H
5#	40	1	HB

composite UV curable materials with dosages of 0%, 10%, 20%, 30%, and 40% were prepared, the properties of which are shown in Table 5: we found that with the addition of HEA can effectively reduce the shrinkage of composite materials. With the increase in the amount of HEA, paint adhesion increases, while pencil hardness decreases slightly. This is because HEA is an acrylate containing hydroxyl groups, and the adhesion to substrates such as glass is very good, so with the increase in the HEA usage, the adhesion of composite materials to substrates such as glass also increases. ARA is a bifunctional UV-curable rosin derivative. Curing can increase the crosslinked density and cohesion strength of the coating. Therefore, the increase in the amount of HEA will lead to a decrease in the hardness of the composite. Considering the two properties of adhesion and pencil hardness, the composite material showed the best performance when the HEA dosage was 20%.

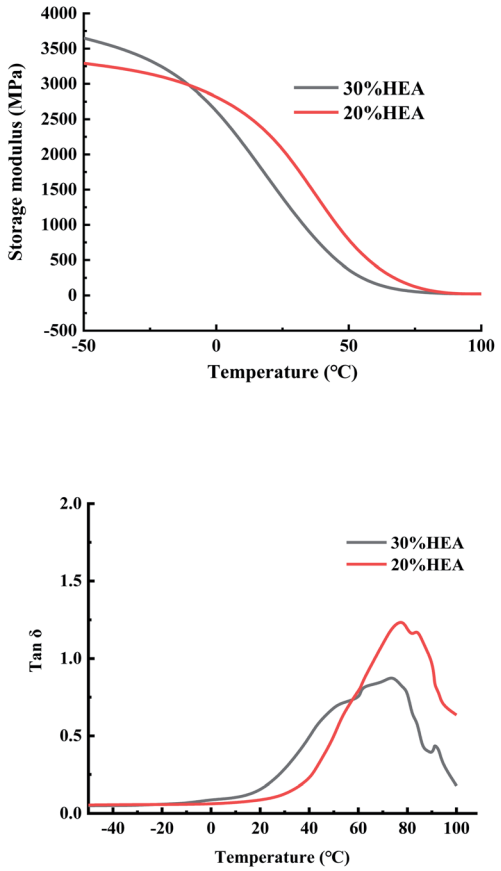

Fig. 6 DMA analysis of composite materials.

3.4.6 Dynamic mechanical analysis of composite materials. In order to analyze the effect of the active diluent content on the dynamic mechanical properties of light-curing composites, the examples of recipes 3# and 4# were taken. As can be seen from Fig. 6, above 0 °C, the composite material containing 20% HEA has a higher storage modulus, which was consistent with the test results of the pencil hardness in Table 5. In contrast, composites containing 20% HEA also have higher vitrification transition temperatures.

3.4.7 Time-double bond conversion curve of composite materials. After calculation, a time-double bond conversion curve for the composites in formula 3# was obtained (Fig. S7†). Due to the high reactivity of the epoxy tung oil derivatives, the double bond conversion rate of the composite material increased sharply at the beginning, and then the conversion rate gradually decreases.

3.4.8 Effect of initiator dosage. The light curing system pays considerable attention to the compatibility of the photoinitiator and the initiation system, and the selection of the appropriate initiator can greatly improve the curing speed and even improve the performance of the cured material. Fig. 7 shows a curing kinetic curve under the two initiation systems of Darocur 1173 and BP/triethanolamine. As can be seen from this figure, at the concentration of the same initiator, the system of BP/triethanolamine as the initiator exhibits a relatively slow reaction speed and a low double bond conversion rate. This phenomenon is caused by the different photolysis mechanisms of the two initiators. Darocur 1173 is a Norrish Type I initiator that performs photolysis directly under the light. The most common is α cleavage. BP belongs to the Noble II type initiator, and the active free radical produced after initiation absorbs active hydrogen and is then terminated.

Under the same amount of the initiator addition, on the one hand, the molecular weight of BP is large, and the mole number of BP actually added is relatively small. On the other hand, the free radicals produced by BP are still inactivated. Therefore, considering that in this system, Darocur 1173 has a better effect than BP initiation.

3.4.9 ATRFT-IR analysis of tung oil matrix composites before and after curing. With bifunctional radical polymerization of epoxy tung oil, 3% mass photo initiator Darocur 1173 was added to investigate the changes in the infrared

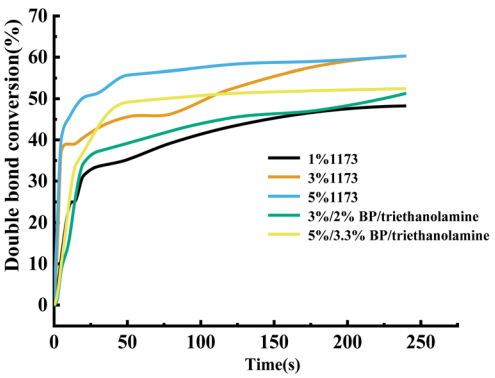

Fig. 7 Effect of initiators on the time-conversion rate.

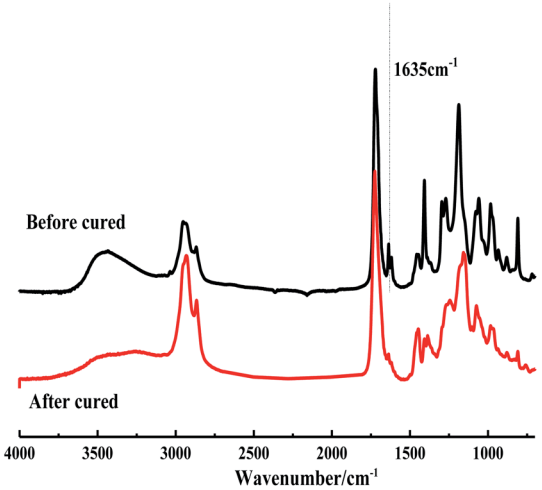

Fig. 8 IR spectra before and after UV curing of tung oil matrix composites.

spectrogram before and after curing. As shown in Fig. 8, the changes in the infrared spectra are mainly the changes in the absorption intensity of the tung oil ester unsaturated double bond absorption peak at 1635 cm^{-1}. After the reaction, the unsaturated double bond basically disappears and the reaction is basically complete.

3.4.10 Effects of ARA/HEA film thickness. In the application of materials, UV curing materials are required to achieve rapid curing. There are two main reasons for this. First, the application process involves the use of high-pressure mercury lamps, the light is powerful, and the continuous irradiation time is too long to make the polymer surface temperature rise too high so that the polymer substances are oxidized. Second, from the perspective of energy saving, it is also necessary to reduce the light exposure time. Therefore, in order to achieve fast curing without affecting the performance of the coating film, the UV curing film must be selected with a suitable thickness. Fig. 9 shows the influence curve of formula 3# on the double bond conversion rate of rosin-based UV-cured coatings at different film thicknesses. As shown in the figure, the film thickness is a parameter of the curing speed. The film thickness increased from 25 μm to 75 μm, with a decrease in the initial double bond conversion, sequentially, and the final conversion decreased slightly. This is because the light intensity decreases with the increase in the illumination depth, so the reaction rate gradually decreases. However, the conversion rate of the final double bond can be improved by extending the reaction time.

3.4.11 Effect of light intensity on curing behavior. Ultraviolet photo initiators produce free radicals during light curing, and the greater the intensity of the active radicals initiated, the faster the reaction. However, when the light intensity reaches a saturation value, the concentration of light is increased, and the concentration of active free radicals cannot be increased. Fig. S8† shows the light curing behaviour of recipe 3# at different light intensities. The two curves show a similar trend, both at the beginning of the reaction conversion rate increased sharply, and the reaction speed slows down when thirty seconds

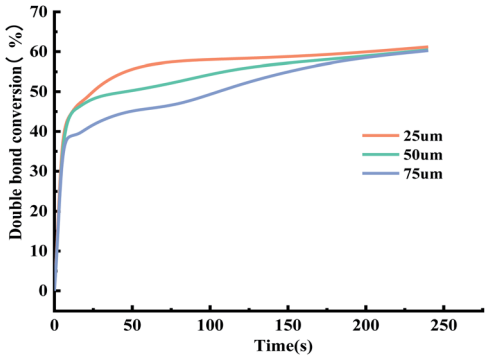

Fig. 9 Effect of film thickness on the time-conversion rate.

were reached, the speed inflection point occurs earlier at high light intensity than at low light intensity, and the final conversion rate at high light intensity is slightly higher than at low light intensity. From the curve in the figure, the greater the light intensity, the higher the concentration of active free radicals, which reflects the faster the light curing speed.

3.5 Characterization of tung oil-based 3D printing AETP resins and products

3.5.1 Flow viscosity. In addition to preparing low-viscosity tung oil-based flexible resins, reactive diluents (TPGDA) are also required to adjust the viscosity of the resin. Samples were configured for testing according to Table 2. Fig. 10 is the flow viscosity–shear rate curve of different formulations, it can be seen that the viscosity of the printed material decreases significantly with the increase in the shear rate, this phenomenon is called shear thinning.[39] The shear thinning effect of AETP-1 is more pronounced than that of the formulas AETP-3 and AETP-2. On the one hand, the higher the content of epoxy tung oil and the lower the TPGDA content, the greater the viscosity of the system. On the other hand, because the benzene ring in the polymer long chain of the system makes the epoxy tung oil unable to move freely; these two reasons lead to the intensification of the phenomenon of shear thinning.[40]

In addition to preventing the pressure of the resin from being severely sheared and thinning caused by the lifting and

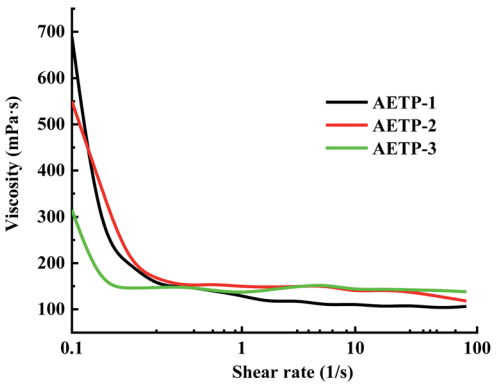

Fig. 10 Flow viscosity–shear rate curves of different formulations.

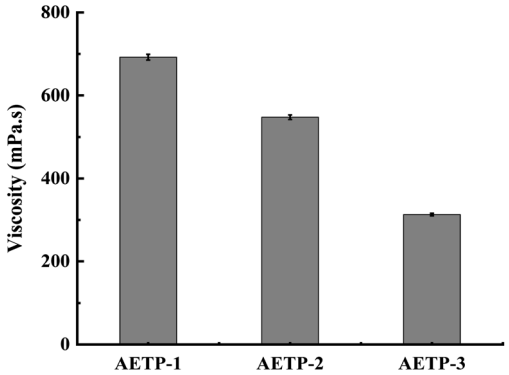

Fig. 11 Viscosity of different formulations at 0.1 s^{-1} shear rate.

moving of the table when printing, it is also necessary to avoid the problem that the resin stick is very large and the flow is poor, resulting in the filling of the bottom printing layer in a timely manner. Therefore, a formulation with a low shear thinning degree, low viscosity, and stable flow should be selected. Compared with the viscosity of the EPIC type resin from a German company of 361.7 mPa s and the NHC02 type resin of a company in Shanghai with 300 mPa s, it can be seen that the viscosity of the 3D printed resin products on the market is about 1000 mPa s or less. As shown in Fig. 11, the viscosity of different formulations at a shear rate of 0.1 s^{-1}, compared with the viscosities of formulation AETP-1, AETP-2, AETP-3, AETP-3, the viscosity reduction was the most significant and could effectively control the viscosity of the system at about 313–548 mPa s, and can be used as the preferred formulation to reduce viscosity.

3.5.2 Determination of exposure time. Following the configuration of the print materials shown in Table 2, testing was performed using the rheometer MCR302, and the results obtained are shown in Fig. S9(a), (b), (c),† representing the energy storage modulus–time curves of AETP-1, AETP-2, AETP-3 for different exposure times, respectively. We can determine the most suitable exposure time for different formulations through the analysis of this curve. Observations in Fig. S6(a)† indicate that in the time of 3 to 4 s, the energy storage modulus of the formulation AETP-1 resin exposed for 3 s, 4 s, and 5 s increased significantly with the increase of time because the free radicals activated by the resin in the print material triggered by the photoinitiator TPO are continuously polymerizing. When the polymerization was close to complete, the energy storage modulus slowly increased and finally stabilized. As the exposure time increased from 3 s to 4 s, the energy storage modulus increased significantly, and the energy storage modulus with an exposure time of 4 s was about 1.61 times that of the exposure time of 3 s. When the exposure time was increased from 4 s to 5 s, the increment of energy storage modulus becomes smaller but still increases, and the most suitable printing exposure time of formulation AETP-1 can be concluded at 4.5 s. Compared with other mass-produced resins at home and abroad, the knowable formulation AETP-1 has a fast printing rate.

3.5.3 Anisotropy and stress–strain curves. Configure the sample according to Table 2, prepare the barbell type test strip

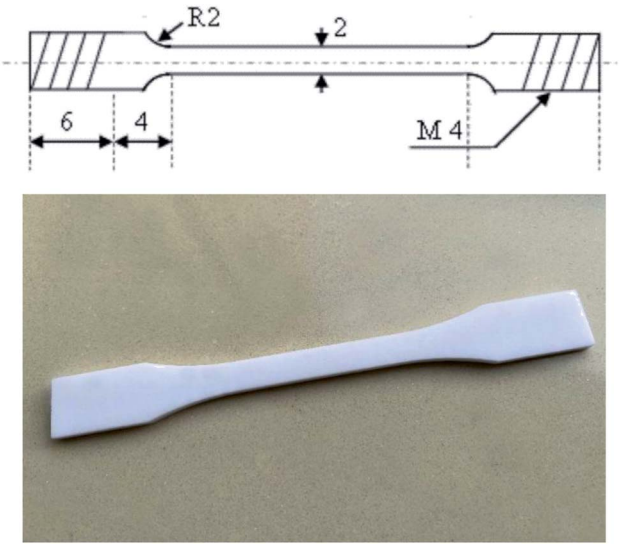

Fig. 12 Barbell type test strip.

according to the size in Fig. 12, and conduct the tensile strength test, Fig. 13 shows the tensile strength of different formulations. We found that formulation AETP-1 had the highest tensile strength after curing, followed by formulation AETP-2 and formulation AETP-3. When the formulation contains a higher dipropylene glycol diacrylate content and lower composite matrix content, the higher the tensile strength of the printed material after molding and curing. This is due to the benzene-like ring structure of dipropylene glycol diacrylate, which makes the resin resistant to greater external stress after curing, has extremely high rigidity and strength, and improves the flexibility of the sample after curing, but also reduces the tensile strength of the sample.[41] Compared to the EPIC resin from a German company with a tensile strength of 16.8 MPa, a WIC100 resin with a tensile strength of 14.8 MPa, and an NHC02 resin from a Shanghai company with a tensile strength of 18 MPa, it can be seen that the formulations AETP-1 and AETP-2 showed better tensile strength.

The stress and strain curves of the specimen being stretched and deformed to break at different times are shown in Fig. 14.

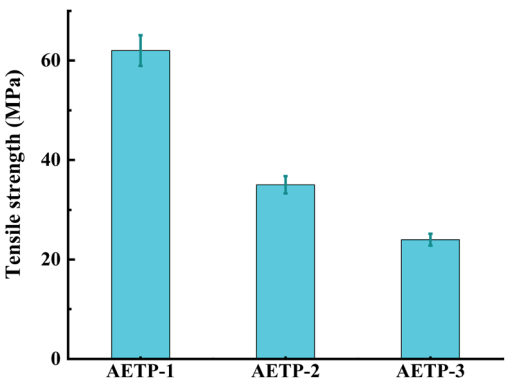

Fig. 13 Tensile strengths of three formulations.

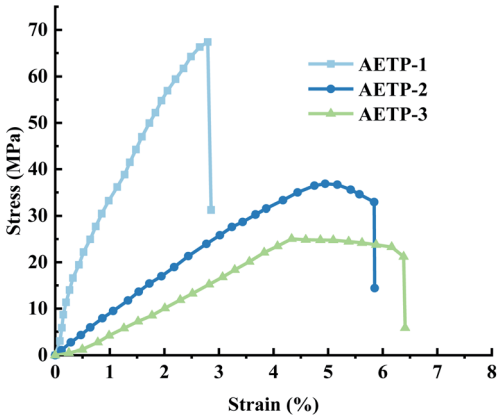

Fig. 14 Stress–strain curves for different formulations.

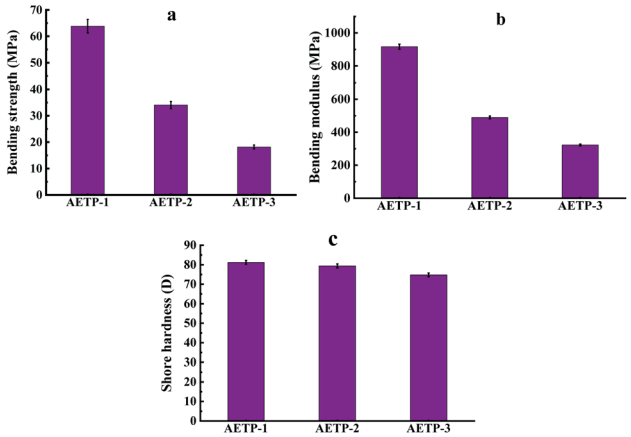

Fig. 16 Flexural strength/flexural modulus/Shore hardness for different formulations.

Formulation AETP-1 was consistent with Hooke's law when stress increases during tension as the strain increases, and fracture occurs when the maximum stress is reached.[42] The material has linear elasticity and the test strip undergoes brittle fracture. The curves for the formulations AETP-2 and AETP-3 are divided into two stages, and the stress increased linearly with the increase in strain at the beginning, which belonged to the linear elastic stage. After reaching the maximum stress, the stress changed nonlinearly with the increase in strain and gradually decreased, which belongs to the shaping and softening stage.[43] This is because when the sample is stretched by external forces, the long chain of polymers will be stretched oriented, and a more obvious yield phenomenon occurred.[44] Compared with the German company's EPIC type resin's elongation at the break of 7.46%, WIC100 type resin elongation was at the break of 6.3%, its flexibility is better than that of the homemade one. Follow-up should also be performed in the aspect of flexibility and toughening. Overall, formulations AETP-1 and AETP-2 have greater tensile strength after curing, while formulations AETP-2 and AETP-3 have better flexibility and toughening effect after curing (Fig. 15).

3.5.4 Analysis of flexural strength/flexural modulus/Shore hardness D. According to Table 2, the samples were configured for bending strength testing. Tables S4–S6† show the bending strength, bending modulus, and Shore hardness of the different formulation samples, and Fig. 16(a)–(c) show the bending strength/bending modulus/Shore hardness of the different formulation samples. We found that the cured sample of formulation AETP-1 has a bending strength of up to 63.84 MPa, which is about 1.87 times greater than that of formulation AETP-2. The flexural modulus of formulation AETP-1 reaches 916.708 MPa, which was approximately 1.86 times that of formulation AETP-2. The bending strength of formulation AETP-2 was 34.073 MPa, which is about 1.87 times that of formulation AETP-3. The flexural modulus of AETP-2 reaches 489.778 MPa, which was about 1.51 times that of formulation AETP-3.

As can be seen from Fig. 16(a) and (b), with the increase in the diacrylate content of dipropylene glycol diacrylate and the decrease of the matrix content of the composite material, the flexural strength and flexural modulus of the resin after curing are significantly increased. It is explained that the increase of benzene ring content in the printing material can improve the bending resistance of the resin after curing, show extremely high rigidity, and resist greater bending stress. Compared with the bending strength of 23 MPa of the EPIC type resin from a German company and the bending strength of 50 MPa of the NHC02 type resin from a company in Shanghai of, it can be seen that formulation AETP-1 and formulation AETP-2 show good tensile strength. As can be seen from Fig. 16(c), the surface hardness of the cured AETP-1 and AETP-2 print materials was excellent, and the Shore hardness could reach about 80 D, without significant differences. The cured formulation AETP-3 showed a slightly weaker Shore hardness (75 D), which was 6.25% lower than that of the other two.

In order to show better-bending resistance and surface hardness after resin light curing, priority should be given to the ratio of the two printing materials of the formulation AETP-1 and AETP-2, which is more conducive to printing precision small components such as gem. This ensures that the components under the table shovel and cleaning process avoid

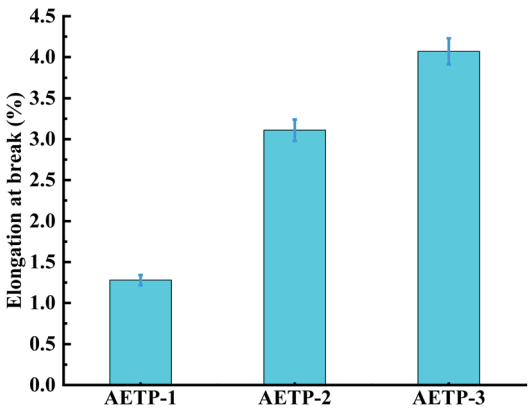

Fig. 15 Elongation at the break for different formulations.

obvious elongation deformation caused by the resin being too flexible.

4. Conclusions

Acrylate-epoxy tung oil polypolymer AETP was prepared from tung oil. The structure of the compound was determined by infrared spectroscopy. Using tung oil matrix composites as prepolymers, a new type of AETP resin suitable for light-curing 3D printing was developed (2-HEMA, TPGDA as active diluent; TPO and Irgacure 1173 as photoinitiators). This resin meets the requirements for use in desktop-grade 3D printers. The prepared tung oil-based 3D printing resin has good mechanical properties and is suitable for the application of ultraviolet curing materials. The prepared 3D printing products have good mechanical properties and thermal properties. The benzene ring in the formulation can effectively improve the performance of 3D printing products. When the AETP content in the resin reached 55%, the tensile strength of the 3D printing product was 63.84 MPa, the hardness was 80 HD, the exposure time was 4.5 s, and the viscosity was 313 mPa s. The results show that UV photo reparation can effectively improve the performance of 3D printed products. The crosslinking density effectively improves the mechanical properties of 3D printing products based on MCPP resin. Tung oil-derived AETP forms a bio-based acrylate that could be a suitable alternative to petrochemical acrylates. This study not only reports a preparation method of photoactive acrylate for light-curing 3D printing but also strongly promotes the application of woody oil biomass resources in light-curing 3D printing, which is of particular significance for the development of sustainable polymers.

Funding

This work was supported by Major Landmark Innovation Demonstration Project, 2019XK2002; Changsha Functional Oil Technology Innovation Center, KH2101007; Hunan Forestry Bureau Outstanding Training Research Project, XLK202108-2.

Author contributions

Zicheng Zhao: methodology, software, formal analysis, investigation, writing—original draft preparation, writing—review, and editing; Hongwu: modification; Xudong Liu: methodology, data curation, writing—original draft preparation, writing—review and editing; Desheng Kang: software; Zhihong Xiao: validation and funding acquisition; Qiquan Lin: conceptualization; Aihua Zhang: methodology, resources, and funding acquisition;

Conflicts of interest

The authors announce that they have no known competing financial interests or personal relationships that could have appeared to influence the work reported in this paper.

Acknowledgements

The authors gratefully appreciate the support of this work by the Hunan Academy of Forestry by providing the necessary facilities.

References

1 I. Volyanskii and I. V. Shishkovsky, *New Trends in 3D Printing*, IntechOpen, 2016, DOI: 10.5772/63565.
2 X. Kuang, D. J. Roach, J. Wu, C. M. D. Hamel, Z. Ding, T. Wang, M. L. Dunn and H. J. Qi, *Adv. Funct. Mater.*, 2019, **29**, 1805290.
3 F. P. W. Melchels, M. A. N. Domingos, T. J. Klein, J. Malda, P. J. Bartolo and D. W. Hutmacher, *Prog. Polym. Sci.*, 2012, **37**, 1079–1104.
4 J. Zhang and P. Xiao, *Polym. Chem.*, 2018, **9**, 1530–1540.
5 D. Chattopadhyay and K. Raju, *Prog. Polym. Sci.*, 2007, **32**, 352–418.
6 M. Sangermano, N. Razza and J. V. Crivello, *Macromol. Mater. Eng.*, 2014, **299**, 775–793.
7 R. D. Farahani, K. Chizari and D. Therriault, *Nanoscale*, 2014, **6**, 10470–10485.
8 C. Williams, A. James, M. P. Chae and D. J. Hunter-Smith, *J. Foot Ankle Res.*, 2015, **8**, O41.
9 B. Zhang, K. Kowsari, A. Serjouei, M. L. Dunn and Q. Ge, *Nat. Commun.*, 2018, **9**, 1831.
10 A. V. Wijk and I. v. Wijk, *3D Printing with Biomaterials: Towards A Sustainable and Circular Economy*, 2015.
11 S. K. Bhatia and K. W. Ramadurai, *3D Printing and Bio-Based Materials in Global Health*, Springer International Publishing AG, 2017.
12 E. M. Fernandes, R. A. Pires, J. F. Mano and R. L. Reis, *Prog. Polym. Sci.*, 2013, **38**, 1415–1441.
13 J. Liu, R. Korpinen, K. S. Mikkonen, S. Willför and C. Xu, *Cellulose*, 2014, **21**, 2587–2598.
14 L. Zhang, Z. Liu, G. Cui and L. Chen, *Prog. Polym. Sci.*, 2015, **43**, 136–164.
15 C. Zhang, T. F. Garrison, S. A. Madbouly and M. R. Kessler, *Prog. Polym. Sci.*, 2017, **71**, 91–143.
16 Q. Wu, Y. Hu, J. Tang, J. Zhang, C. Wang, Q. Shang and W. Lei, *ACS Sustainable Chem. Eng.*, 2018, **6**, 8340–8349.
17 N. Thanamongkollit, K. R. Miller and M. D. Soucek, *Prog. Org. Coat.*, 2012, **73**, 425.
18 X. Yang, S. Li, J. Xia, J. Song, K. Huang and M. Li, *Ind. Crops Prod.*, 2015, **63**, 17.
19 B. Liang, J. Zhao, G. Li, Y. Huang, Z. Yang and T. Yuan, *Ind. Crops Prod.*, 2019, **138**, 111585.
20 L. Man, Y. Feng, Y. Hu, T. Yuan and Z. Yang, *J. Cleaner Prod.*, 2019, **241**, 118341.
21 Z. Yang, X. Ye, J. Huang, B. Liang and T. Yuan, *Mater. Rep.*, 2018, **32**, 3831–3838.
22 M. Li, S. Li, J. Xia, C. Ding, M. Wang, L. Xu, X. Yang and K. Huang, *Mater. Des.*, 2017, **122**, 366.
23 D. Wu, B. Chen, R. Sun and G. Liu, *J. Anal. Appl. Pyrolysis*, 2017, **128**, 143–155.

24 D. H. Qi, K. Yang, D. Zhang, B. Chen, Q. Wei and C. H. Zhang, *Renewable Energy*, 2017, **113**, 1201.
25 H. Li, Y. Cui, Z. Li, Y. Zhu and H. Wang, *Prog. Org. Coat.*, 2018, **115**, 164.
26 M. Desroches, M. Escouvois, R. Auvergne, S. Caillol and B. Boutevin, *Polym. Rev.*, 2012, **52**, 38.
27 M. Y. Shah and S. Ahmad, *Prog. Org. Coat.*, 2012, **75**, 248–252.
28 M. Li, S. Li, J. Xia, C. Ding, M. Wang, L. Xu, X. Yang and K. Huang, *Mater. Des.*, 2017, 366–375.
29 S. Levine, H. J. Stevenson and P. W. Kabler, *Arch. Biochem. Biophys.*, 1953, **45**, 65–73.
30 M. Wang, J. Xia, J. Jiang, S. Li, K. Huang, W. Mao and M. Li, *Polym. Degrad. Stab.*, 2016, **133**, 136–143.
31 J. Seetula, K. Kalliorinne and J. Koskikallio, *J. Photochem. Photobiol., A*, 1988, **43**, 31–41.
32 V. V. Korshak, S. L. Sosin, G. L. Slonimskii, A. A. Askadskii, L. I. Zakharkin, A. I. Kovredov, B. A. Antipova, K. A. Bychko and Z. S. Shaugumbekova, *Pergamon*, 1986, **28**, 265–271.
33 X. Liu, F. P. Bouxin, J. Fan, V. L. Budarin, C. Hu and J. H. Clark, *ChemSusChem*, 2020, **13**, 4296–4317.
34 H. Wu, M. Lin, J. Wang, C. Wang and F. Chu, *Chem. Ind. For. Prod.*, 2009, **30**, 43–46.
35 X. Wang, *Master thesis*, Guangdong University of Technology, 2019.
36 Y. Zhong, *Master thesis*, Guangdong University of Technology2018.
37 K. Li, *Master thesis*, South China University of Technology, 2018.
38 G. Lu and W. Liu, *Journal of Henan University of Technology (Natural Science Edition)*, 2019, **40**, 26–31.
39 N. Moszner and U. Salz, *Prog. Polym. Sci.*, 2001, **26**, 535–576.
40 X. Chen, J. Zhang, W. Xu and J. Liu, *Polym. Bull.*, 2019, **6**, 68–70.
41 J. Hu, P. Fu, H. x. Ma and W. Sang, *Mod. Paint Finish.*, 2012, **15**, 1–3.
42 X. Gao, W. Yang, B. Chi, Z. Jiao and J. Tan, *China Plastics*, 2015, **29**, 73–76.
43 F. Wang, *Master thesis*, South China University of Technology, 2012.
44 W. Zhang, P. Du, G. Jiang, L. Sun and S. Song, *Modern Machinery*, 2008, 93–94.